High-Frequency Radars: Beamforming Calibrations Using Ships as Reflectors*

X. FLORES-VIDAL

Instituto de Investigaciones Oceanológicas, Universidad Autónoma de Baja California, Ensenada, Baja California, Mexico

P. FLAMENT

Department of Oceanography, School of Ocean and Earth Science and Technology, University of Hawaii at Manoa, Honolulu, Hawaii

R. DURAZO

Facultad de Ciencias Marinas, Universidad Autónoma de Baja California, Ensenada, Baja California, Mexico

C. CHAVANNE

Institut des Sciences de la Mer de Rimouski, Université du Québec à Rimouski, Rimouski, Québec, Canada

K.-W. GURGEL

Institut für Meereskunde, Universität Hamburg, Hamburg, Germany

(Manuscript received 16 May 2012, in final form 2 October 2012)

ABSTRACT

Linear array antennas and beamforming techniques offer some advantages compared to direction finding using squared arrays. The azimuthal resolution depends on the number of antenna elements and their spacing. Assuming an ideal beam pattern and no amplitude taper across the aperture, 16 antennas in a linear array spaced at half the electromagnetic wavelength theoretically provide a beam resolution of 3.5° normal to the array, and up to twice that when the beam is steered within an azimuthal range of 60° from the direction normal to the array. However, miscalibrated phases among antenna elements, cables, and receivers (e.g., caused by service activities without recalibration) can cause errors in the beam-steering direction and distortions of the beam pattern, resulting in unreliable ocean surface current and wave estimations. The present work uses opportunistic ship echoes randomly received by oceanographic high-frequency radars to correct an unusual case of severe phase differences between receiver channels, leading to a dramatic improvement of the surface current patterns. The method proposed allows for simplified calibrations of phases to account for hardware-related changes without the need to conduct the regular calibration procedure and can be applied during postprocessing of datasets acquired with insufficient calibration.

1. Introduction

High frequency radars (HFRs) have become a powerful tool for remotely measuring ocean surface currents, waves, and wind. HFRs have the ability to sample coastal areas (3–20 km from shore) up to ~350 km offshore, depending on the working frequency. The transmitted electromagnetic signal propagates along the conductive sea surface and is backscattered by the

* School of Ocean and Earth Science and Technology Contribution Number 8581.

Corresponding author address: Xavier Flores-Vidal, Instituto de Investigaciones Oceanológicas, Universidad Autónoma de Baja California, Carretera Tijuana–Ensenada km 103, Ensenada BC 22860, Mexico.
E-mail: floresx@uabc.edu.mx

DOI: 10.1175/JTECH-D-12-00105.1

resonant ocean's surface gravity waves with exactly half the wavelength transmitted (Crombie 1955). Two strong peaks, each surrounded by sidebands, characterize the most energetic signals in the Doppler spectrum of the radar echo. These first-order Bragg lines are Doppler shifted (a fraction of a hertz above and below the transmitted signal) by Bragg resonant surface gravity waves and ocean currents propagating radially toward or away from the radar. The Doppler shift due to the resonant ocean waves can be computed from the dispersion relation for ocean gravity waves, yielding the speed of the radial currents. Second-order scattering generates the sidebands. There are several techniques to compute wave parameters from these second-order echoes, including hydrodynamic and electromagnetic interactions (Hasselmann 1971), as well as transfer functions and inversion of a nonlinear integral wave equation (Barrick et al. 1977). Retrieving the ocean's wave parameters require second-order sidebands with large signal-to-noise ratio (SNR) (Teague et al. 1997; Gurgel et al. 1999). Furthermore, a modulation of the signals scattered by ocean waves in response to the wind has been used to estimate wind direction and, in some cases, wind speed near the ocean surface (Long and Trizna 1973; Stewart and Barnum 1975; Shearman and Wyatt 1982; Shen et al. 2012).

Among the techniques used to estimate the radial distance of the backscattering patches of the ocean surface, the most common is the use of a frequency-modulated continuous wave (FMCW) as transmitted signal. FMCW is a continuous linearly swept chirp. The range resolution is given by $c/2B$, where c is the speed of light and B is the chirp bandwidth of the transmitted signal.

Common techniques to estimate the direction of the backscattering targets are direction finding and beamforming. Both are postprocessing digital techniques that require calibrations of gain and phase responses for each channel. Without calibrations, these techniques yield spurious directions and poor azimuthal resolution.

Changes in the surroundings, such as construction of buildings, roads, or power lines, affect the propagation of the electromagnetic waves (Krim and Viberg 1996) and introduce phase variations that affect both beamforming and direction finding, and therefore the azimuthal mapping of currents and waves. Ideally, transponder calibrations (Fernandez et al. 2003, 2006) should be run as often as possible to account for changes that could affect the electromagnetic propagation. However, neither bistatic nor transponder calibrations were performed for the case study presented here: the Gulf of Tehuantepec, Mexico. The cables linking the antennas to the receivers were dramatically changed in length after flooding, long-term sun exposure, mishandling, and damage by nesting sea turtles.

To circumvent these problems, ship echoes were used successfully to recover the phase response for the 16-antenna linear array. The data and method are described in section 2, and the resulting improvements are illustrated in section 3. Section 4 summarizes the results.

2. Data and methods

From 2005 to 2008, two HFR sites were installed along the Gulf of Tehuantepec coast. The sites consisted of 16 equally spaced antennas at a working frequency of 16.3 MHz with 150-kHz bandwidth, yielding 1-km radial resolution and a maximum range of ~120 km. The azimuthal resolution scales as λ/D (rad), where λ is the electromagnetic wavelength (18.4 m at 16.3 MHz) and $D = d(N - 1)$ (the aperture or length of the N-antenna array). For $N = 16$ and $d = \lambda/2$ spacing, $D = 138$ m yields a resolution of ~7° (0.13 rad). This theoretical azimuthal resolution is only achieved for the direction normal to the array and for an ideal beam pattern. Resolution degrades by a factor of 2 at beam-steering angles of ±60°, a practical limit; it is also affected by the window applied to reduce sidelobes and by distortions due to noncalibrated gains and phase differences between the array elements.

In addition to damage to the cables, four undocumented antenna channel swapping rendered the original phase calibrations useless. Such problems are usually corrected by conducting transponder runs at known azimuth and ranges, which unfortunately could not be conducted during this deployment. Instead, we use ships of opportunity as sources of echoes with sufficient strength.

In contrast to transponder runs, the ship echo method needs to identify echoes with sufficient signal-to-noise ratio (>20 dB) in the backscatter Doppler spectra (Gurgel and Schlick 2005); furthermore, the azimuth of the ships are unknown, even though the phase shift of the ship signal across the aperture should be a linear function of the antenna number, with a slope dependent on ship azimuth. We visually examined the Doppler spectra to locate about 100 echoes spread over 3 years of HFR data. With a sufficient number of ship echoes (preferably spread in azimuth to cover the beam-steering range), the problem can be treated as an overestimated system of equations, solving for the antenna phases and the ships' azimuth as a minimum mean-squared error problem.

Let the phases at each antenna be referenced to the phase at antenna 1 (i.e., antenna 1 phases are assumed 0).

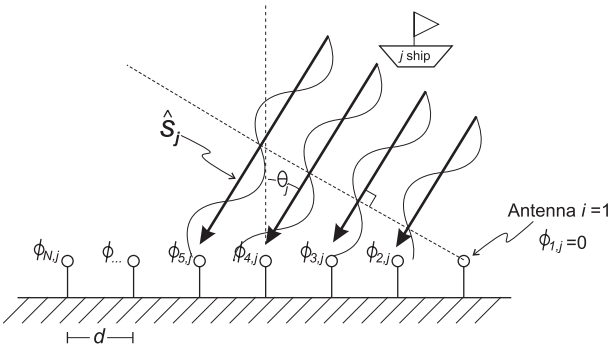

FIG. 1. Geometry of the antenna elements and electromagnetic wave reflection or echo (bold arrows or $\hat{S}_j$) of a ship. The phase differences among the antennas ($\phi_{i,j}$) and the angle (θ_j) from the normal to the antenna array are sketched.

The problem's unknowns are the $N-1$ phase error $\hat{\phi}_i$ between antenna i and antenna 1 ($\hat{\phi}_1 = 0$), and the M angles from the normal to the array θ_j of the ship echoes (see Fig. 1). We solve the problem by minimizing the sum of squared errors as shown:

$$P = \sum_{j=1}^{M} \sum_{i=2}^{N} [\phi_{i,j} - (i-1)\hat{S}_j - \hat{\phi}_i]^2, \tag{1}$$

where $\phi_{i,j}$ is the phase measured at antenna i from the ship echo j and $\hat{S}_j = 2\pi\, d/\lambda \sin(\theta_j)$, where d is the antenna spacing. Solving for each antenna's phase, the solution is given by

$$\frac{\partial P}{\partial \hat{\phi}_i} = -2 \sum_{j=1}^{M} [\phi_{i,j} - (i-1)\hat{S}_j - \hat{\phi}_i] = 0, \quad i = 2, \ldots, N, \tag{2}$$

or

$$M\hat{\phi}_i + (i-1) \sum_{j=1}^{M} \hat{S}_j = \sum_{j=1}^{M} \phi_{i,j} \quad i = 2, \ldots, N. \tag{3}$$

Solving for each ship's echo phase, the solution is given by

$$\frac{\partial P}{\partial \hat{S}_j} = -2 \sum_{i=2}^{N} [\phi_{i,j} - (i-1)\hat{S}_j - \hat{\phi}_i](i-1) = 0, \quad j = 1, \ldots, M, \tag{4}$$

or

$$\sum_{i=2}^{N} \hat{\phi}_i (i-1) + \hat{S}_j \sum_{i=2}^{N} (i-1)^2 = \sum_{i=2}^{N} (i-1)\phi_{i,j} \quad j = 1, \ldots, M. \tag{5}$$

Equations (3) and (5) can be expressed in matrix form by

$$\mathbf{XB} = \mathbf{Y}, \tag{6}$$

where

$$\mathbf{B} = \begin{bmatrix} \hat{\phi}_2 \\ \vdots \\ \hat{\phi}_N \\ \hat{S}_1 \\ \vdots \\ \hat{S}_M \end{bmatrix}, \quad \mathbf{Y} = \begin{bmatrix} \sum_{j=1}^{M} \phi_{2,j} \\ \vdots \\ \sum_{j=1}^{M} \phi_{N,j} \\ \sum_{i=2}^{N} (i-1)\phi_{i,1} \\ \vdots \\ \sum_{i=2}^{N} (i-1)\phi_{i,M} \end{bmatrix}$$

and

$$\mathbf{X} = \begin{bmatrix} M & \cdots & 0 & 1 & \cdots & 1 \\ \vdots & \ddots & \vdots & \vdots & \vdots & \vdots \\ 0 & \cdots & M & (N-1) & \cdots & (N-1) \\ 1 & \ldots & (N-1) & \alpha_N & \cdots & 0 \\ \vdots & \ldots & \vdots & \vdots & \ddots & \vdots \\ 1 & \ldots & (N-1) & 0 & \cdots & \alpha_N \end{bmatrix}, \tag{7}$$

where $\alpha_N = \sum_{i=2}^{N} (i-1)^2$.

Matrix $\mathbf{X}$ has a size of $M + N - 1$ but a rank of $M + N - 2$; therefore, $\mathbf{X}$ is singular and the least squares problem does not have a unique solution. A null vector is

$$\boldsymbol{\eta} = \begin{bmatrix} 1 \\ \vdots \\ N-1 \\ -1 \\ \vdots \\ -1 \end{bmatrix} \tag{8}$$

and the solutions are

$$B_\alpha = B_o + \alpha\boldsymbol{\eta}, \tag{9}$$

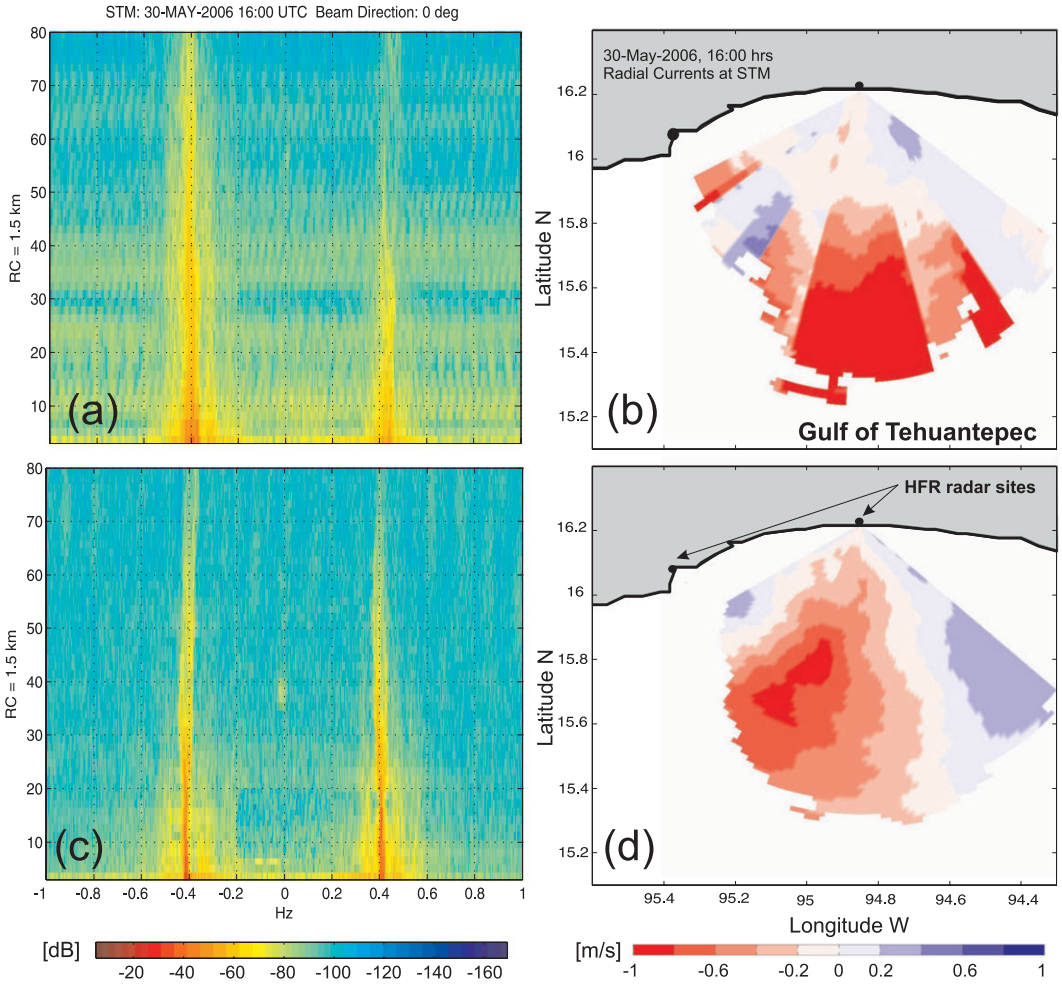

FIG. 2. (a) Backscatter power vs Doppler frequency and range for a beam steered normal to the antenna linear array. (b) Corresponding radial currents mapped to a polar grid. Radial currents (>0 toward the HFR) have an erratic azimuthal distribution due to uncalibrated phases. (c),(d) As in (a),(b), but after the phase corrections have been applied.

where B_o is a particular solution not proportional to the null vector and α is an arbitrary real number. The singularity of $\mathbf{X}$ arises from the fact that the cost function P in (1) cannot discriminate between a linear trend in the phase errors $\hat{\phi}_i = (i-1)\alpha$ and a mean ship bearing $\hat{S}_j = -\alpha$.

A particular solution is

$$B_o = \mathbf{X}^{\dagger}\mathbf{Y}, \tag{10}$$

where $\mathbf{X}^{\dagger}$ is the Moore–Penrose pseudoinverse of $\mathbf{X}$. This particular solution is not necessarily the solution closest to the actual phase errors and ship bearings. To find the latter, one has to determine the appropriate value of α (see the appendix for more details).

3. Results

Although we applied this method for the two HFR sites installed in the Gulf of Tehuantepec (Fig. 2d), we report in this paper only the eastern site [named Santa Maria (STM)], since it was the most dramatic case of phase errors. Time invariant phases were assumed, since neither constructions, buildings, power lines, roads, nor major changes were experienced on the site. Figure 2a shows a typical power spectrum in the frequency-range domain for a beam steered at 0° (normal to the array). First-order peaks are well defined (SNR > 20 dB) for both negative and positive Doppler-shifted frequencies, but second-order Bragg scatter can be barely seen, blurred by a frequency-independent interference (with SNR < 20 dB) pattern at every ≈10 range cells. Figure 2b shows

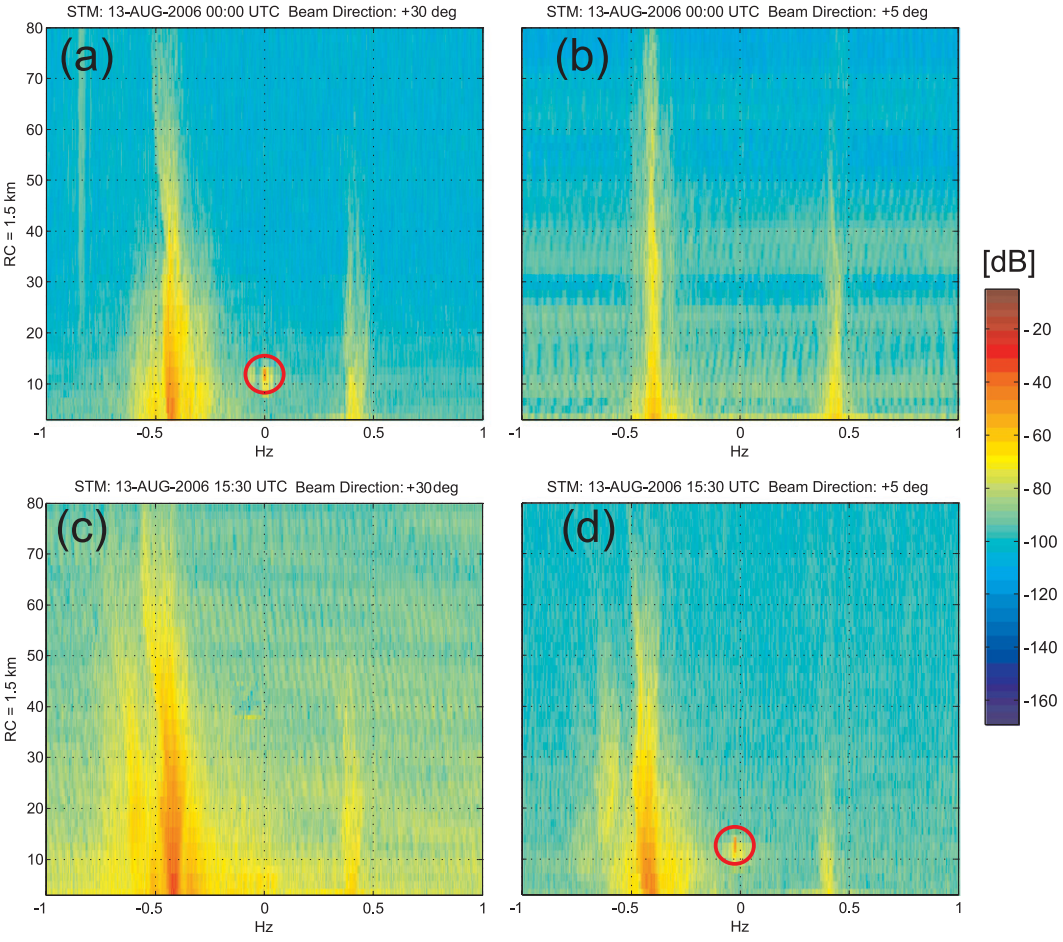

FIG. 3. Backscatter power vs Doppler frequency and range for a beam steered at (left) +30° and (right) +5°, from 14-min (2048 samples) acquisitions at (top) 0000 and (bottom) 1530 UTC 13 Aug 2006. Potential ship echoes are indicated by red circles.

the corresponding radial currents mapped to a polar grid. There is evidence of misplaced azimuthal sectors, resulting from distorted beam patterns due to uncalibrated phases.

We used ship echoes to estimate the phase differences between antenna elements. Visual identification of potential ship echoes was made for a large number of Doppler spectra. Some conditions have to be satisfied for a spectral peak to be correctly identified as a ship echo. First, the echo must be localized in range, azimuth, and Doppler frequency. Echoes near zero Doppler frequency correspond to either ships moving only in the azimuthal direction and through the same range cell or not moving at all. Echoes at Doppler frequency different from zero correspond to ships with nonzero radial velocity, which may be found at different range cell or azimuth through time. A ship moving at the same radial speed as ocean currents has its echo overlaid on the first-order Bragg lines, rendering its detection difficult or impossible.

Figure 3a shows a ship echo (with SNR $>$ 20 dB) located at zero Doppler frequency and centered at range cell 12 (18 km offshore). This ship was detected with a bearing of +30° (185°N) at 0000 UTC 13 August 2006. Figure 3b shows that at the same instant but at a bearing of +5° the ship echo is not discernible. By 1530 UTC the same day, another ship was detected moving at the same range cell 12 but at a bearing of +5° (Fig. 3d), while no echo was discernible anymore at +30° (Fig. 3c). About 100 such ship echoes (with SNR $>$ 20 dB) satisfying the required conditions were identified. Phases at each receiver channel were extracted for the corresponding range cell and Doppler frequency. Finally, the overestimated set of equations was solved in the least squares sense (see section 2 and the appendix) to find the phase differences between antenna elements.

TABLE 1. Phase error and standard (std) errors, as determined by 10 000 bootstrap realizations of a matrix of 10, 50, and 100 ships' echoes. All phases are referenced to antenna 1.

Antenna	Phase error and std error using 10 ships	Phase error and std error using 50 ships	Phase error and std error using 100 ships
2	33 ± 5	38 ± 5	40 ± 0.5
3	9 ± 10	13 ± 2	13 ± 0.75
4	−12 ± 15	−2 ± 7	0 ± 1
5	10 ± 15	7 ± 4	5 ± 2
6	−10 ± 20	1 ± 15	2 ± 2.5
7	4 ± 20	2 ± 14	4 ± 3
8	−60 ± 42	−23 ± 14	−15 ± 4
9	−68 ± 40	−48 ± 15	−32 ± 5
10	−59 ± 30	−65 ± 10	−65 ± 4
11	−91 ± 30	−98 ± 10	−100 ± 5
12	−102 ± 32	−105 ± 10	−115 ± 4
13	−101 ± 35	−104 ± 12	−114 ± 5
14	−72 ± 50	−48 ± 12	−39 ± 5
15	−80 ± 35	−52 ± 12	−49 ± 5
16	−15 ± 10	−10 ± 4	−8 ± 0.5

Table 1 shows the phases among the antennas as estimated by Eq. (10) for 10, 50, and 100 ships. The standard errors were obtained by a stochastic procedure in which the ship's matrix was randomly resampled 10 000 times (by drawing with replacement, allowing duplications and omissions) while all the statistics parameters were collected (a well-known method called "bootstrap"; Efron and Gong 1983). The bootstrap method not only allowed us to obtain the standard error of the recovered phase error but also allowed us to estimate the precision in azimuth of the resulting beamforming. Figure 4 shows the mean phase differences and standard errors (light gray, gray, and dark gray shadows for 10, 50, and 100 ships, respectively) as determined from 10 000 bootstrap realizations for a matrix of 10, 50, and 100 ships' echoes (dotted, dashed, and solid line, respectively). The estimated error is well behaved and improves as the number of echoes increases. For matrices composed of 50 echoes, the standard phase errors ranged from 5° to 15°, while matrices with 100 echoes the phase error was reduced to 0.5°–5°. It is worth noting that the mean phase values lies within the error range while increasing the number of ship echoes.

The data presented in Figs. 2a,b are shown in Figs. 2c,d after calibrating the receiver antennas with the values estimated from Eq. (10) and reported in Table 1 (bootstrapped mean for 100 ships). Bragg lines are narrower and stronger, and the weak interference pattern previously observed over the whole frequency domain has disappeared, suggesting improvement of the SNR and more precise beamforming. As expected, the resulting radial currents (Fig. 2d) have a better pattern that is in good agreement with common regional oceanographic features for this HFR site, where currents are strongly wind driven toward the southwest with two compensating countercurrents (northward) on each side of the Tehuantepec wind axis (Flores-Vidal et al. 2011).

A statistical way to assess the data quality is to compute cross correlations between radial currents from the two radar sites: it must be close to 1 for those ranges where both systems measure almost the same current component and −1 on the baseline between the two

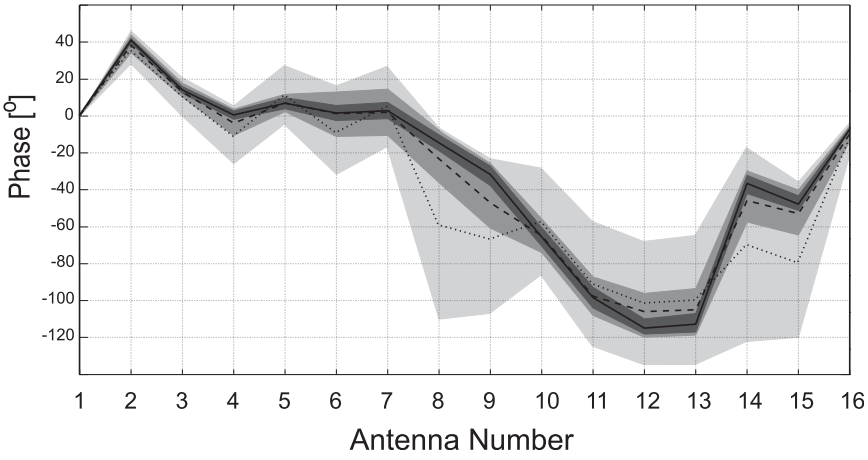

FIG. 4. Phase error (line) and standard errors (shadow), as determined by 10 000 bootstrapped realizations for a matrix of 10 (light gray shadow and dotted line), 50 (gray shadow and dashed line), and 100 (dark gray shadow and solid line) ships' echoes. All phases are referenced to antenna 1.

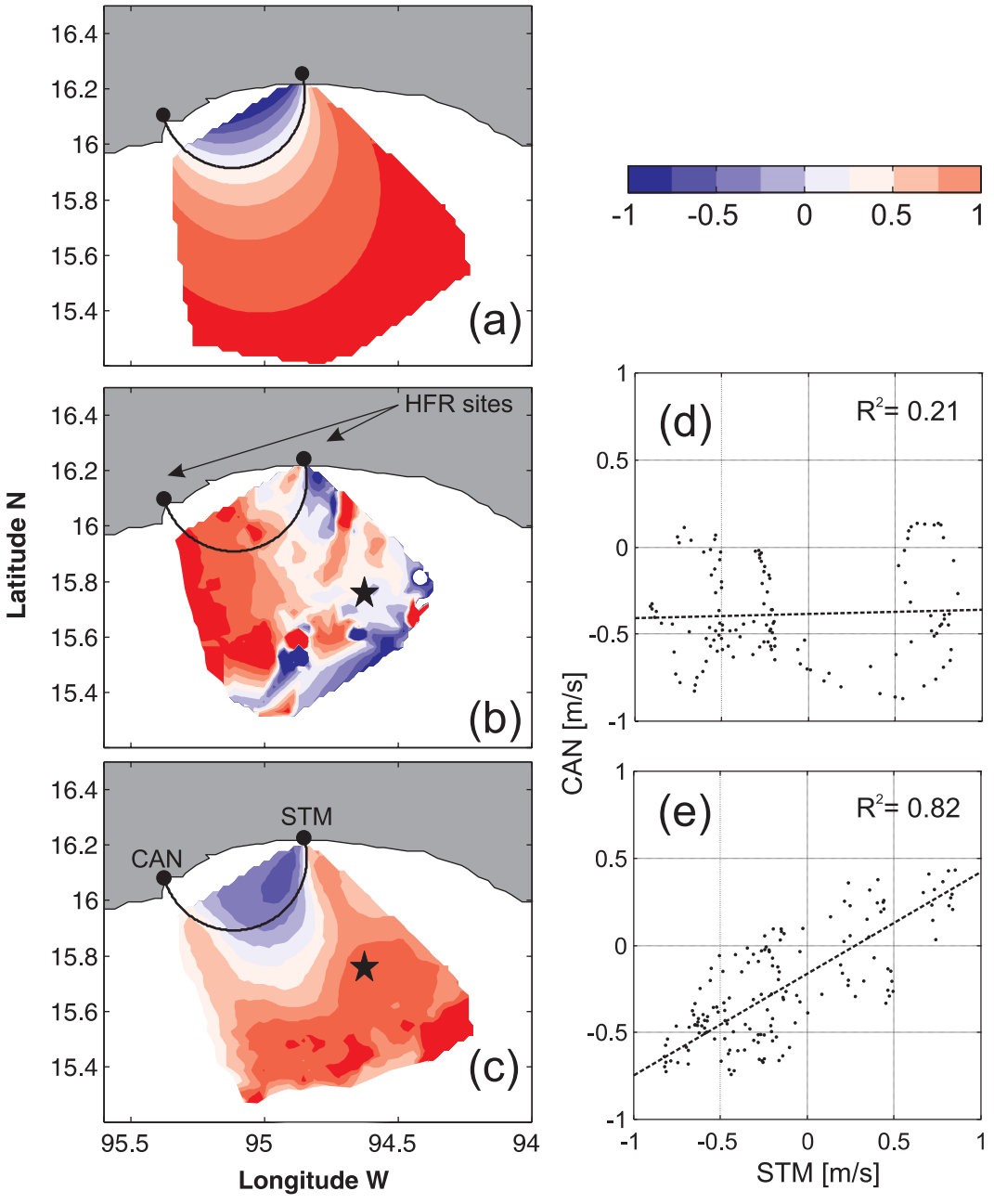

FIG. 5. Radial currents' correlation between the two HFR sites. (a) Theoretical spatial pattern plotted as the cosine of the angle between radial lines. (b) Correlation spatial pattern for 2 months of miscalibrated radial currents. (c) Correlation spatial pattern after phase corrections have been applied. Linear regression and correlation coefficient for a single grid point (as marked by the star); (d) before corrections and (e) after corrections.

sites, where the current component is opposed (Chavanne et al. 2007). A theoretical spatial pattern is given by the cosine of the angle between radials originating at both sites (Fig. 5a). Figure 5b shows the cross-correlation pattern for ≈2 months of radial currents obtained with uncalibrated phases; it bears no resemblance to the theoretical pattern. Figure 5c obtained from the same ≈2 months of radial currents, but with calibrated phases, is close to the theoretical pattern. Figures 5d,e also show the scatterplot of the radial currents before and after the corrections, extracted at the point marked by a star symbol, at which the two sites can be expected to have

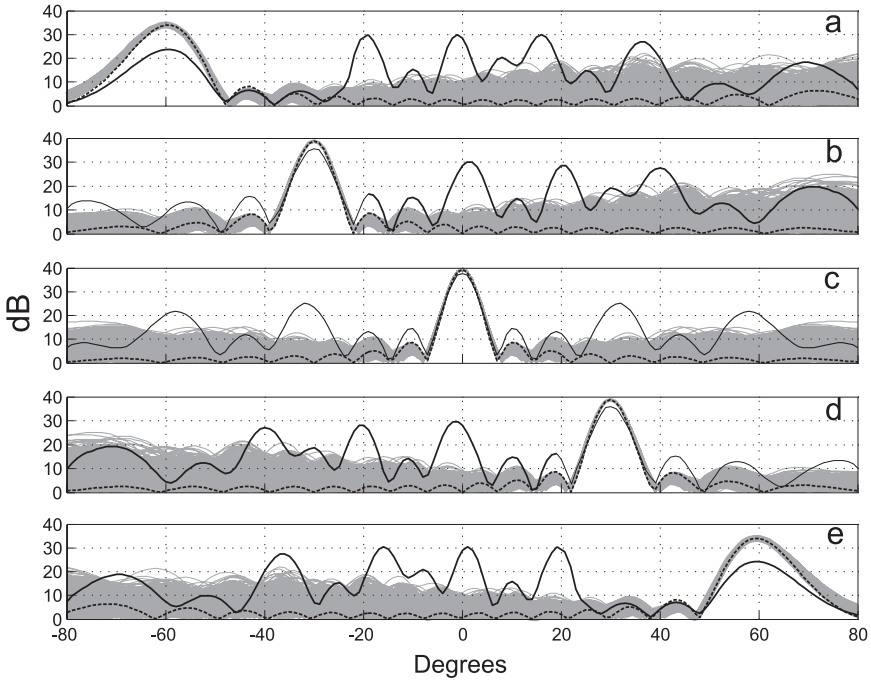

FIG. 6. Theoretical beamforming patterns steering at (a) −60°; (b) −30°; (c) 0°, i.e., normal to the array; (d) 30°; and (e) 60°. Solid black line is the beamforming before phase correction. Dashed line is the ideal or zero phase-error beamforming. Thin gray lines are the beamforming patterns after phase correction, as estimated by the 10 000 bootstrapped realizations from a matrix of 100 ships' echoes.

a cross-correlation approaching 1 for the correct beamforming.

The dramatic improvement of the radial currents' correlation suggests an important improvement of the beamforming pattern. To evaluate this, Fig. 6 shows the theoretical beamforming pattern (steerings of −60°, −30°, 0°, 30°, and 60°) as estimated by synthetically inducing the erroneous phase values originally in the data (solid black line), the beamforming pattern for zero phase error (ideal case) among the receivers (dashed black line), and the beam-forming pattern after correcting the erroneous phase values as estimated by each of the 10 000 bootstrapped realizations (thin gray lines). Before correction for the erroneous phases, a decreased gain of the main beam (the steering direction) and increased sidelobes can be seen, worsening as the steering angle augments. Sidelobes of −30° and 30° beam steering (Figs. 6b,d) are about 5 dB lower than the main beam, while for −60° and 60° (Figs. 6a,e) the main beam can no longer be identified in terms of its gain. After the corrections (light gray lines) the degradation of the main beam at wide angles (Figs. 6a,e) is in good agreement with the theoretical beam-pattern degradation (dashed black line) and the sidelobes remain well below (15–20 dB) the main beam at all the steering angles. Beamforming quality not only involves strong gain of the main beam and negligible sidelobes, but precision on azimuth is also required. Figure 7 shows histograms that represent the precision of the five steering angles presented on Fig. 6 for the 10 000 bootstrapped realizations. For the direction normal to the array (0°, Fig. 6c), the bootstrapped beamformed estimations had a standard deviation of 0.5°; at ±30° (Figs. 6b,d), the standard deviation was 1.1°, while at wide angles (i.e., ±60°, Figs. 6a,e) it was 1.8°. The corresponding averages, −60.09, −30.04, 0, 29.95, and 59.9, show that the azimuthal biases are negligible.

4. Concluding remarks

Miscalibrated antenna channel phases for HFRs can lead to erroneous current and wave estimations due to erroneous beam-steering angles. This work presents a simple but robust statistical method to estimate phase differences between antenna channels. The results show significant improvements of the beamforming patterns, with a precision of ±1° and an SNR of ≈20 dB (between

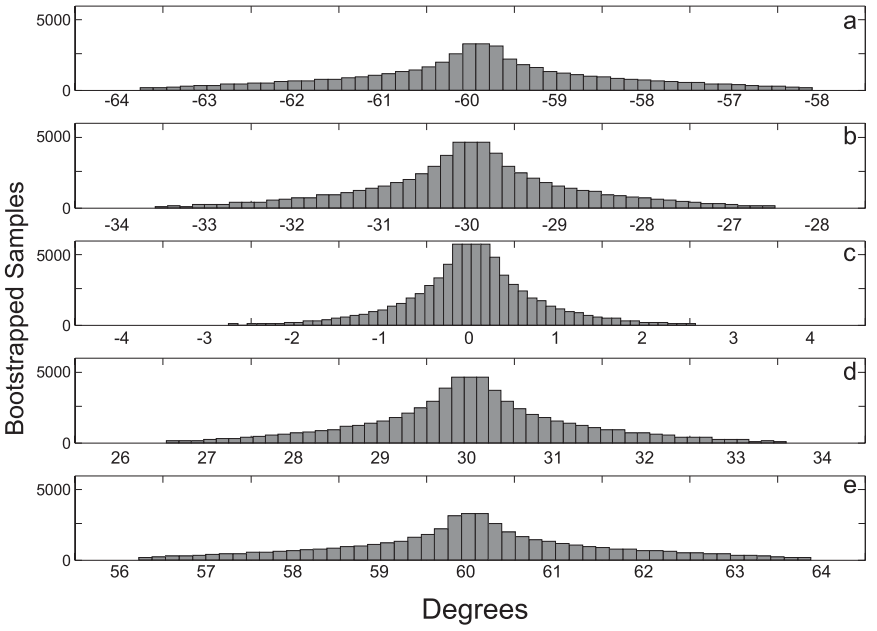

FIG. 7. Histograms of the maximum gain, as estimated by 10 000 bootstrapped realizations, for beamforming steerings at (a) −60°; (b) −30°; (c) 0°, i.e., normal to the array; (d) 30°; and (e) 60°. The histogram is a representation of the steering precision.

the main beam and sidelobes) leading to a dramatic improvement of the radial current estimations. Additionally, an increase of the SNR improves the detection of second-order sidebands, hence the estimation of wave spectrum parameters. Furthermore, since this method only requires finding ship echoes in the Doppler spectra, it could be applied as often as necessary to account for time variance due to changes in the surroundings (i.e., new roads, buildings, electric lines, etc.) that may affect the electromagnetic propagation and the phases at the receiver channels. This technique can potentially reduce or even eliminate the need for transponder runs to calibrate HFRs.

Acknowledgments. Xavier Flores-Vidal was supported by CONACyT (Mexican Council of Science), Ph.D. scholarship and international stipend 207824. The POGO International Fellowship Program provided a supplementary stipend. P. Flament was supported by the Department of Homeland Security and by the State of Hawaii. R. Durazo was supported by CONACyT Grants U40822-F and 85108. Universidad Autónoma de Baja California contributed with Internal Programs 321 and 363. Universidad del Mar (UMAR) and Secretaría de Marina (SEMAR) provided personnel during the HFR installation and logistics. We thank Louis Marié, D. Fernandez, and anonymous reviewers for their helpful suggestions, especially on the singularity of the least-square problem matrix.

APPENDIX

Testing Methods with Synthetic Data

For linear equally spaced antenna receive arrays, the determination of an exact value of α [see Eq. (9)] is not possible without prior knowledge about phase errors or ship bearings. However, some considerations can be made to approach a reasonably good estimate.

Here, we used four synthetic datasets of phases measured on each of the 16 equally separated antennas on a linear array, each antenna separated by $\lambda/2$. A total of 50 ship echoes $\hat{S}_j$ was randomly generated, with a mean angle of 30° normal to the linear array. Phase errors $\hat{\phi}_i$ relative to the first antenna were randomly generated and detrended, while a second set of phase errors was created, adding a linear trend. To generate a second set of ship bearings symmetrically distributed at right angles to the array, the resulting were demeaned. Thus, four sets of synthetic phase errors and ship bearings were combined to artificially create four sets of measured phases, namely,

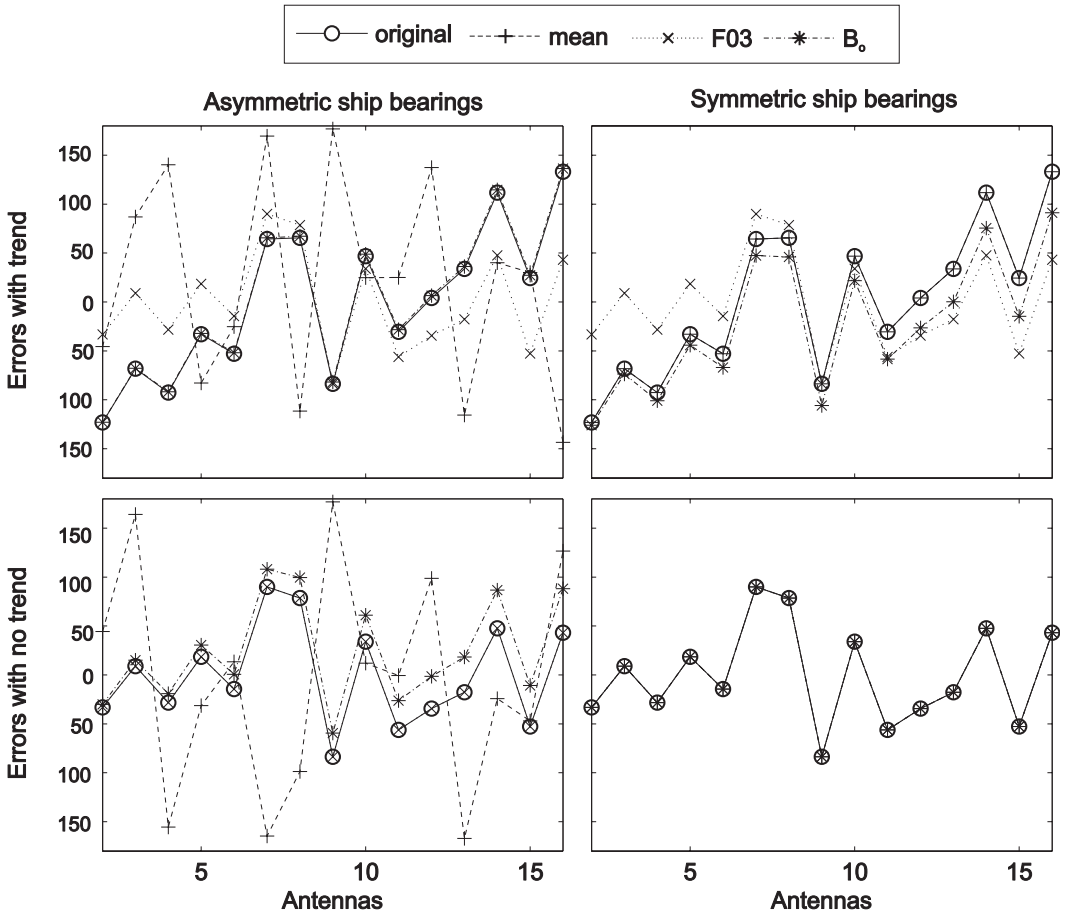

FIG. A1. Synthetically generated phase errors (o). Retrieval of these errors are shown for the cases of a simple average (+); the method of Fernandez et al. (2003), called F03 (×); and the pseudoinverse method, called B_o (*). Phase errors were generated (top) with and (bottom) without a linear trend across the antenna receive array. Ship bearings were (left) asymmetrically and (right) symmetrically distributed normal to the receive array.

$$\phi_{i,j} = (i-1)\hat{S}_j + \hat{\phi}_i,$$

where $\phi_{i,j}$ is the phase measured at antenna i from ship echo j.

In the special case when ship bearings $\hat{S}_j$ are symmetrically distributed relative to the direction normal to the receive array, the mean of $\hat{S}_j$ should tend to zero as the number of ship echoes tends to infinity, enabling to uniquely determine α. The solution for this case is quite simple, and phase errors $\hat{\phi}_i$ are obtained by the average of measured phases over all ship echoes [right column of panels in Fig. A1 and Eq. (3) with $\sum_{j=1}^{M} \hat{S}_j = 0$]. Although this simple averaging yields the best estimate of phase errors for the case, it can also seriously bias the results under asymmetry of $\hat{S}_j$ (left column of panels in Fig. A1). When this occurs, the particular solution B_o [Eq. (10)] produces better results, differing only from the actual phase errors by a relatively small linear trend (see Fig. A1).

Another special case is when a linear trend in phase errors does not exist. Since the first $N-1$ elements of η [see Eqs. (8) and (9)] arise from a pure linear trend, one can uniquely determine α so the first $N-1$ elements of B_o lack a linear trend. The solution in this case is that obtained by Fernandez et al. (2003). However, when a linear trend in phase errors does exist, the method fails to retrieve it since it erroneously assigns the trend to the mean ship bearing (top row of panels in Fig. A2). In this case, the particular solution of B_o yields better results since the trends in phase errors are close to the real slopes.

Our conclusion is that without prior knowledge of phase errors or ship bearings, the particular solution of B_o [Eq. (10)] yields reasonably good results in all cases. This is the solution we have chosen here.

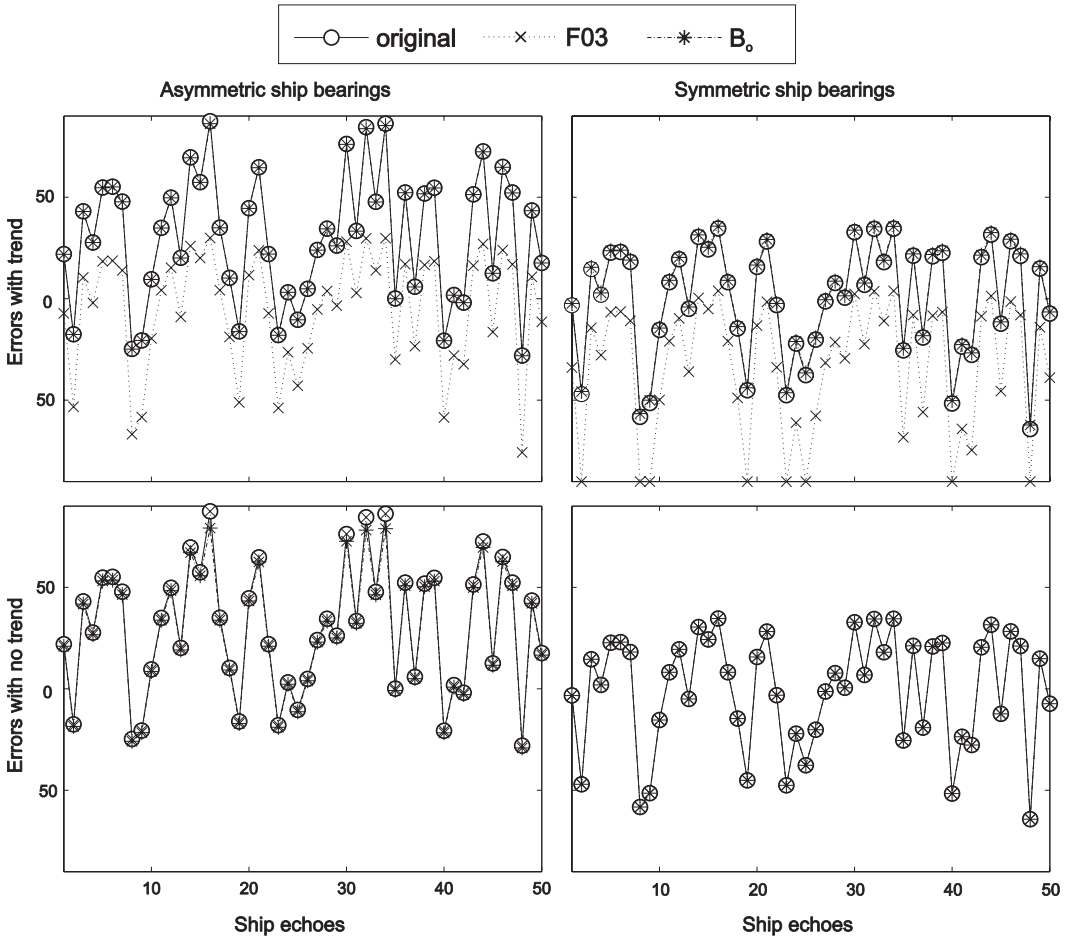

FIG. A2. As in Fig. A1, but for bearings of the synthetically generated ship echoes (o).

REFERENCES

Barrick, D. E., M. W. Evans, and B. L. Weber, 1977: Ocean surface currents mapped by radar. *Science,* **198,** 138–144.

Chavanne, C., I. Janeković, P. Flament, P.-M. Poulain, M. Kuzmić, and K.-W. Gurgel, 2007: Tidal currents in the northwestern Adriatic: High-frequency radio observations and numerical model predictions. *J. Geophys. Res.,* **112,** C03S21, doi:10.1029/2006JC003523.

Crombie, D. D., 1955: Doppler spectrum of sea echo at 13.56 Mc./s. *Nature,* **175,** 681–682, doi:10.1038/175681a0.

Efron, B., and G. Gong, 1983: A leisurely look at the bootstrap, the jacknife and the cross-validation. *Amer. Stat.,* **37,** 36–48.

Fernandez, D. M., J. Vesecky, and C. Teague 2003: Calibration of HF radar systems with ships of opportunity. *Proc. Int. Geoscience and Remote Sensing Symp.,* Toulouse, France, IEEE, 4271–4273.

——, ——, and ——, 2006: Phase correction of small-loop HF radar system receive arrays with ships of opportunity. *IEEE J. Oceanic Eng.,* **31,** 919–921.

Flores-Vidal, X., R. Durazo, C. Chavanne, and P. Flament, 2011: Coastal circulation in the absence of wind in the Gulf of Tehuantepec, Mexico: High-frequency radio observations. *Cienc. Mar.,* **37,** 493–512.

Gurgel, K.-W., and T. Schlick, 2005: HF radar wave measurements in the presence of ship echoes - Problems and solutions. *IEEE Oceans,* **2,** 937–941.

——, G. Antonischki, H.-H. Essen, and T. Schlick, 1999: Wellen Radar (WERA): A new ground-wave HF radar for ocean remote sensing. *Coastal Eng.,* **37,** 219–234.

Hasselmann, K., 1971: Determination of ocean wave spectra from Doppler radio return from the sea surface. *Nature,* **229,** 16–17.

Krim, H., and M. Viberg, 1996: Two decades of array signal processing research: The parametric approach. *IEEE Signal Process. Mag.,* **6,** 67–94.

Long, A. E., and D. B. Trizna, 1973: Mapping of North Atlantic winds by HF radar sea backscatter interpretation. *IEEE Trans. Antennas Propag.,* **21,** 680–685.

Shearman, E. D. R., and L. R. Wyatt, 1982: Dekametric radar for surveillance of sea-state and oceanic winds. *J. Navig.,* **35,** 397–410.

Shen, W., K.-W. Gurgel, G. Voulgaris, T. Schlick, and D. Stammer 2012: Wind-speed inversion from HF radar first-order backscatter signal. *Ocean Dyn.,* **62,** 105–121, doi:10.1007/s10236-011-0465-9.

Stewart, R. H., and J. R. Barnum, 1975: Radio measurements of oceanic winds at long ranges: An evaluation. *Radio Sci.,* **10,** 853–857.

Teague, C., J. Vesecky, and D. Fernandez, 1997: HF radar instruments, past to present. *Oceanography,* **10,** 40–44.